

Internally Generated Predictions Enhance Neural and Behavioral Detection of Sensory Stimuli in an Electric Fish

Highlights

- Negative images enhance neural coding of prey-like stimuli
- Negative images enhance behavioral detection of prey-like stimuli
- Disrupting synaptic plasticity impairs neural and behavioral detection performance

Authors

Armen G. Enikolopov, L.F. Abbott,
Nathaniel B. Sawtell

Correspondence

ns2635@columbia.edu

In Brief

Stable and accurate perception requires combining sensory input with predictions based on past experience. Using electric fish as a model system, Enikolopov et al. demonstrate improvements in neural coding and behavioral detection of external stimuli due to internally generated predictions.



Internally Generated Predictions Enhance Neural and Behavioral Detection of Sensory Stimuli in an Electric Fish

Armen G. Enikolopov,³ L.F. Abbott,^{1,2} and Nathaniel B. Sawtell^{1,4,*}

¹Department of Neuroscience, Zuckerman Mind Brain Behavior Institute, Columbia University, New York, NY 10027, USA

²Department of Physiology and Cellular Biophysics, Columbia University, New York, NY 10027, USA

³Department of Biological Sciences, Columbia University, New York, NY 10027, USA

⁴Lead Contact

*Correspondence: ns2635@columbia.edu

<https://doi.org/10.1016/j.neuron.2018.06.006>

SUMMARY

Studies of cerebellum-like circuits in fish have demonstrated that synaptic plasticity shapes the motor corollary discharge responses of granule cells into highly-specific predictions of self-generated sensory input. However, the functional significance of such predictions, known as negative images, has not been directly tested. Here we provide evidence for improvements in neural coding and behavioral detection of prey-like stimuli due to negative images. In addition, we find that manipulating synaptic plasticity leads to specific changes in circuit output that disrupt neural coding and detection of prey-like stimuli. These results link synaptic plasticity, neural coding, and behavior and also provide a circuit-level account of how combining external sensory input with internally generated predictions enhances sensory processing.

INTRODUCTION

The notion that internally generated predictions of the sensory consequences of behavior play vital roles in sensory processing and motor control has a long history (Grüsser, 1986). Seminal behavioral experiments performed in fish and flies in the 1950s suggested that corollary discharge signals cancel inappropriate reflexes that would otherwise be triggered by sensory reafference from voluntary movements (Sperry, 1950; von Holst and Mittelstaedt, 1950). Although fixed gating or generalized suppression of sensory responses by corollary discharge has been demonstrated in a variety of systems (Krasne and Bryan, 1973; Poulet and Hedwig, 2007; Richmond and Wurtz, 1980; Roberts and Russell, 1972; Zipser and Bennett, 1976), such mechanisms seem insufficient in cases in which the effects of a motor command are complex, of long duration, or vary over time (e.g., due to growth, fatigue, or injury). von Holst and others posited that the nervous system learns and stores negative images that are highly specific to the sensory consequences of particular motor acts (von Holst, 1954). Studies of cerebellum-like struc-

tures in three separate groups of fish have provided compelling neural correlates of such negative images and have elucidated their synaptic, cellular, and circuit mechanisms at a level of detail that has thus far not been possible in other systems (but see Brooks et al., 2015; Kim et al., 2015; Leinweber et al., 2017). Rather than cancelling specific reflexes, negative images in electrosensory systems are hypothesized to play a more general function, namely, to cancel self-generated sensory input so that unpredictable, behaviorally relevant stimuli can be processed more effectively (Bell et al., 1997a; Bell, 2001; Bodznick et al., 1999). The present study takes advantage of unique features of the passive electrosensory system of weakly electric mormyrid fish to directly test this hypothesis.

Mormyrid fish, as well as a number of non-electrogenic fish, use a passive electrosensory system to detect small, low-frequency electric fields generated by invertebrate prey (Bodznick and Montgomery, 2005). However, detecting these signals is more complex for mormyrids because, at the same time, they employ an electro-motor system for both navigation and communication that involves the repeated generation of large pulsed electric fields known as electric organ discharges (EODs). Each EOD pulse sets the highly sensitive electroreceptors of the passive system into a ringing pattern of activation lasting 100–200 ms (Bell and Russell, 1978), as long as the typical interval between successive EOD pulses. Thus, downstream circuits of the passive electrosensory system face the challenge of pulling out small prey-related signals from ongoing, large-amplitude, EOD-induced firing rate modulations in electroreceptor afferents (see Figure 1 for an illustration of this problem). Moreover, since the frequency content of prey-evoked responses overlaps with that of EOD-evoked responses (Bell and Russell, 1978; Wilkens and Hofmann, 2005; Engelmann et al., 2010), temporal filtering is likely insufficient to solve this problem. Nevertheless, studies of foraging behavior in mormyrid fish have demonstrated that the passive electrosensory system plays a role in prey detection even when other sensory modalities, including the active electrosensory system, are also used (von der Emde and Bleckmann, 1998).

Although it is easy to imagine how cancelling the effects of the EOD through the generation of negative images could enhance sensory processing (Figure 1), there are numerous reasons why such a scheme might fail to explain prey detection. For example, if the EOD saturates the electroreceptors, subtracting



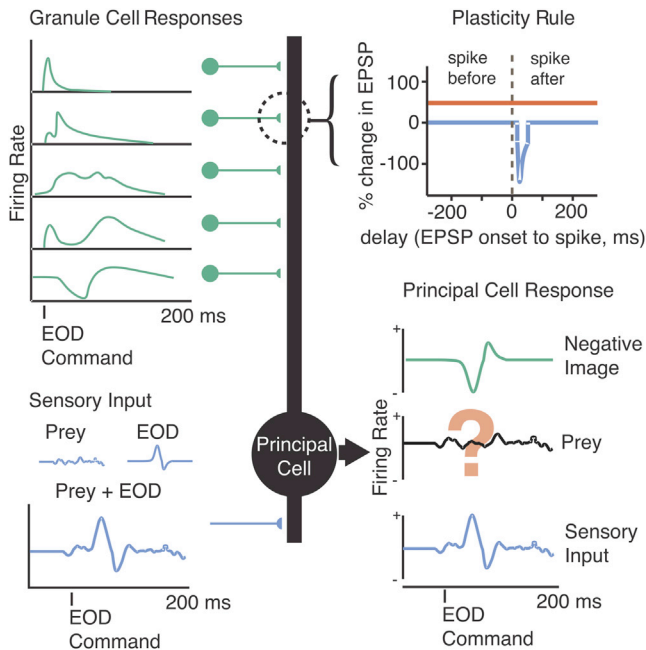


Figure 1. Schematic Illustrating Hypothesized Role of Negative Images in Enhancing Neural Coding of External Stimuli

ELL principal cells (center, black) receive sensory input via electroreceptors (lower left, blue) along with centrally originating motor corollary discharge input via granule cells (upper left, green). The sensory input contains behaviorally relevant signals related to external objects, such as prey, contaminated by the response to the fish's own EOD. Previous results have provided evidence for negative images (lower right, green) formed by anti-Hebbian plasticity consisting of associative synaptic depression (upper right, blue) and non-associative synaptic potentiation (upper right, red) acting on a temporally diverse set of granule cell corollary discharge inputs (upper left, green). A major remaining question is whether such mechanisms are actually sufficient to allow principal cells to detect tiny prey-like signals despite interference due to the fish's EOD (lower right).

a negative image would not be sufficient to recover signals related to external stimuli. Other nonlinear properties of neurons in the electrosensory lobe (ELL) might prevent the simple subtraction process schematized in Figure 1 from being effective, or noise associated with such a subtraction might swamp tiny signals related to prey. Alternatively, non-plastic mechanisms, rather than negative images, might play dominant roles in minimizing the effects of the EOD. Such mechanisms could include spatial filtering (Bodznick and Montgomery, 1992; Montgomery, 1984; Montgomery and Bodznick, 1993) or reductions in neuronal gain (Bastian, 1986; Rotem et al., 2007; Schneider et al., 2014).

Here we report on a series of experiments that addresses these issues and provides—to our knowledge—the first direct evidence that negative images enhance the neural coding and behavioral detection of external electrosensory stimuli. We also use pharmacological manipulations of synaptic plasticity in the ELL to provide support for a mechanistic model linking granule cell temporal representations, spike-timing-dependent plasticity, and negative image formation (Bell et al., 1997c; Kennedy et al., 2014; Roberts and Bell, 2000).

RESULTS

ELL Neurons Respond to Prey-like Stimuli despite Self-Generated Interference

Past studies of mormyrid fish have focused on characterizing negative images and their mechanisms but have never directly tested whether ELL principal neurons can detect external electrosensory stimuli in the presence of self-generated electrosensory input caused by the EOD. We recorded extracellular action potentials from electroreceptor afferent fibers terminating within the first central stage of passive electrosensory processing, known as the ventrolateral zone (VLZ) of the ELL. At the same time, we delivered small, low-frequency electrical stimuli via a dipole electrode positioned in the water near the electroreceptor innervated by the recorded fiber (Figure 2A). Such localized electrical stimuli mimic the electrical fields generated by the fish's invertebrate prey (Chacron et al., 2003; Doiron et al., 2003). In our preparation, neuromuscular paralysis blocks the EOD (the electric organ is a modified muscle), but the fish is unanesthetized and continues to spontaneously emit the motor command that would discharge the electric organ at rates of 3–5 Hz. After each spontaneously emitted EOD motor command (Figure 2B, green lines), we delivered a short electrical pulse that mimics the fish's EOD (see STAR Methods). In other experiments (Figures 3, 4, and 7), we took advantage of this same setup to probe responses to corollary discharge in isolation from electrosensory input by turning the EOD mimic off or to probe the response to electrosensory input in isolation from corollary discharge by delivering the EOD mimic independently of the command.

Consistent with previous reports, electroreceptor afferents exhibit highly regular action potential firing at rates around 50 Hz in the absence of stimulation (Bell, 1982; Engelmann et al., 2010). As can be seen in the traces in Figure 2B, the EOD mimic evoked large firing rate modulations that masked responses to the prey-like stimulus. An offline digital subtraction of the average response to the EOD revealed a reliable underlying encoding of the prey-like stimulus (Figure 2B, dashed line). This observation is important because it rules out the possibility (mentioned in the Introduction) that the EOD prevents afferents from encoding prey-like signals entirely, for example, by saturating their responses.

Identical experiments were performed while recording from principal cells in the VLZ. There are two main classes of ELL principal cells, termed E and I cells. Both are glutamatergic neurons that convey the output of the ELL to higher stages of electrosensory processing in the midbrain (Bell, 1982) (see STAR Methods). E cells, like electroreceptor afferents, increase their firing rates when the voltage outside the electroreceptor is positive, while I cells increase their firing rates when the voltage outside the electroreceptor is negative (Figure S1). In contrast to electroreceptor afferents, firing rate modulations in E and I cells due to prey-like stimuli are larger than the effects of the EOD mimic as can be seen in the example traces (Figures 2C and 2D).

Standard receiver operating characteristic (ROC) analysis was used to quantify these results (Dayan and Abbott, 2001). Such analysis confirmed that, in the presence of the EOD, detection of a prey-like stimulus based on afferent firing rate is poor over a wide range of stimulus amplitudes (Figures 2E and 2H, solid

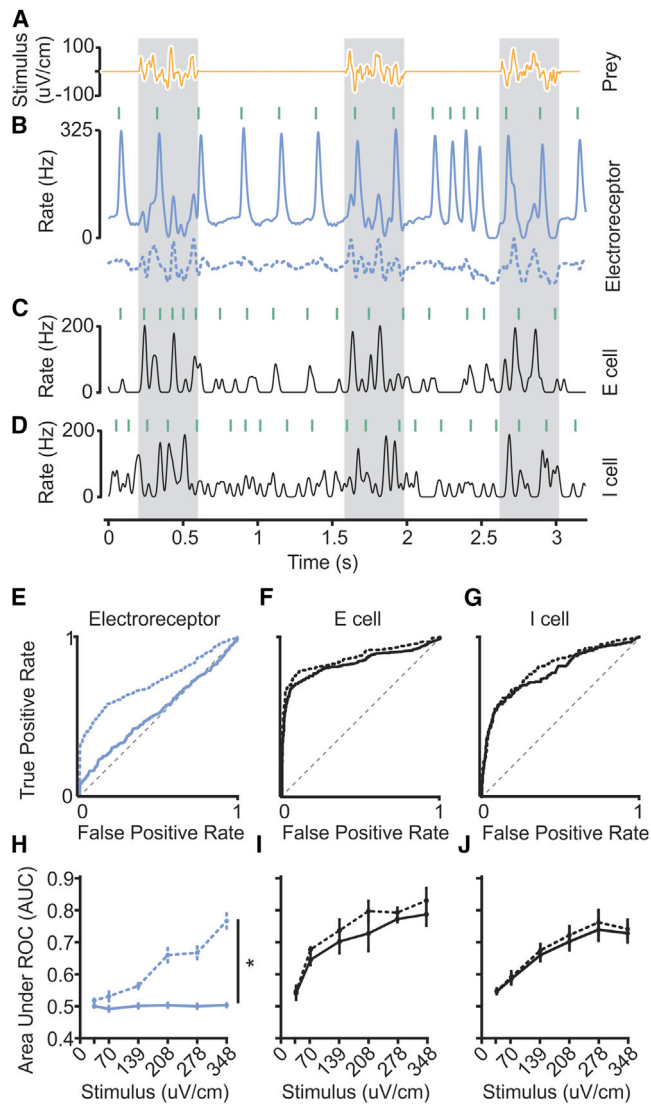


Figure 2. Accurate Detection of Prey-like Stimuli in the ELL despite Self-Generated Interference

(A) Three repetitions of a prey-like stimulus consisting of 400 ms presentations of 5–20 Hz band-passed noise.

(B) Smoothed firing rate of an example electroreceptor afferent before (solid line) and after (dashed line) offline subtraction of the average response of the afferent to the EOD. Green lines indicate the times of EOD commands emitted spontaneously by the fish. An EOD mimic pulse (0.2 ms duration) was delivered 4.5 ms after each EOD command.

(C and D) Smoothed firing rates of example E (C) and I (D) cells in response to a prey-like stimulus (stimulus amplitude and waveform same as used for B).

(E) Quantification of prey-like stimulus detection for the example electroreceptor afferent in (B). ROC curve was calculated based on the peak firing rate in 100 ms periods following the EOD. Gray dashed line indicates chance detection. Solid line indicates prey detection performance in the presence of the EOD. Area under ROC curve (AUC) (unsubtracted) = 0.53. Dotted line indicates detection performance after subtracting the average response to the EOD (dashed line in B). AUC (subtracted) = 0.72.

(F) Quantification of prey-like stimulus detection for the example E cell in (C). AUC (unsubtracted) = 0.84. AUC (subtracted) = 0.87.

(G) Quantification of prey-like stimulus detection for the example I cell in (D). AUC (unsubtracted) = 0.78. AUC (subtracted) = 0.81.

lines). An offline subtraction of the average response to the EOD dramatically improved detection performance in afferents (Figures 2E and 2H, dashed lines). Detection performance in E and I cells is far better than that observed in electroreceptor afferents over a wide range of stimulus amplitudes, presumably due to cancellation of the effects of the EOD (Figures 2F, 2G, 2I, and 2J, solid lines). This result was not sensitive to details of the ROC analysis, such as the size of the analysis windows (Figure S2). Furthermore, offline subtraction of EOD effects in E and I cells yields only small improvement in their detection performance (Figures 2F, 2G, 2I, and 2J, dashed lines), consistent with the hypothesis that EOD effects are already subtracted by negative images. Together, these results show (1) that the EOD is a substantial source of self-generated interference for the passive electrosensory system of mormyrids and (2) that this interference is almost completely removed at the first central stage of processing in the ELL.

An important consideration for evaluating the function of negative images is the relative strength of electroreceptor responses evoked by prey versus those evoked by the EOD. We sought to confirm that our experiments were representative of natural conditions in this regard. We compared the strength of electroreceptor afferent responses evoked by artificial prey-like stimuli to those evoked by actual prey (a live blackworm) (Figure S3). In the presence of a worm, we observed increased variation in the normally highly regular afferent firing rates. Large firing rate modulations were sometimes observed, presumably due to spontaneous movements of the worm, which brought it very near to the pore of the electroreceptor innervated by the recorded afferent. Given the steep falloff of electrical dipole fields with distance (Bodznick and Montgomery, 2005), a strong dependence of neural response magnitude on the exact location of the prey relative to the electroreceptor is expected. A comparison of the magnitude of firing rate variations in the presence of worms to those induced by artificial prey-like stimuli indicate that actual prey are capable of inducing firing rate modulations as large or larger than those used in the present study.

Improvements in Neural Detection of Prey-like Stimuli due to Negative Images

Although the results in Figure 2 show a dramatic improvement in prey detection performance in E and I cells compared to electroreceptor afferents, they do not directly establish whether or to what extent this improvement is the result of negative images. Two approaches were devised to test this. The first takes advantage of our ability to decouple the EOD from the motor command

(H) Summary of detection performance for electroreceptor afferents ($n = 21$) across a range of stimulus amplitudes before (solid line) and after (dashed line) offline subtraction of the effects of the EOD. Mean AUC across stimulus intensities for electroreceptor afferents ($n = 21$) was greater after subtracting the effect of the EOD, $p < 0.0001$, one-tailed Wilcoxon signed rank test. Statistically significant differences are indicated by asterisks.

(I) Summary of detection performance for E cells ($n = 8$). Mean AUC (unsubtracted) across stimulus intensities was greater for E cells than for afferents, $p < 0.0001$, one-tailed Wilcoxon rank-sum test.

(J) Summary of detection performance for I cells ($n = 22$). Mean AUC (unsubtracted) across stimulus intensities was greater for I cells than for afferents, $p < 0.0001$, one-tailed Wilcoxon rank-sum test.

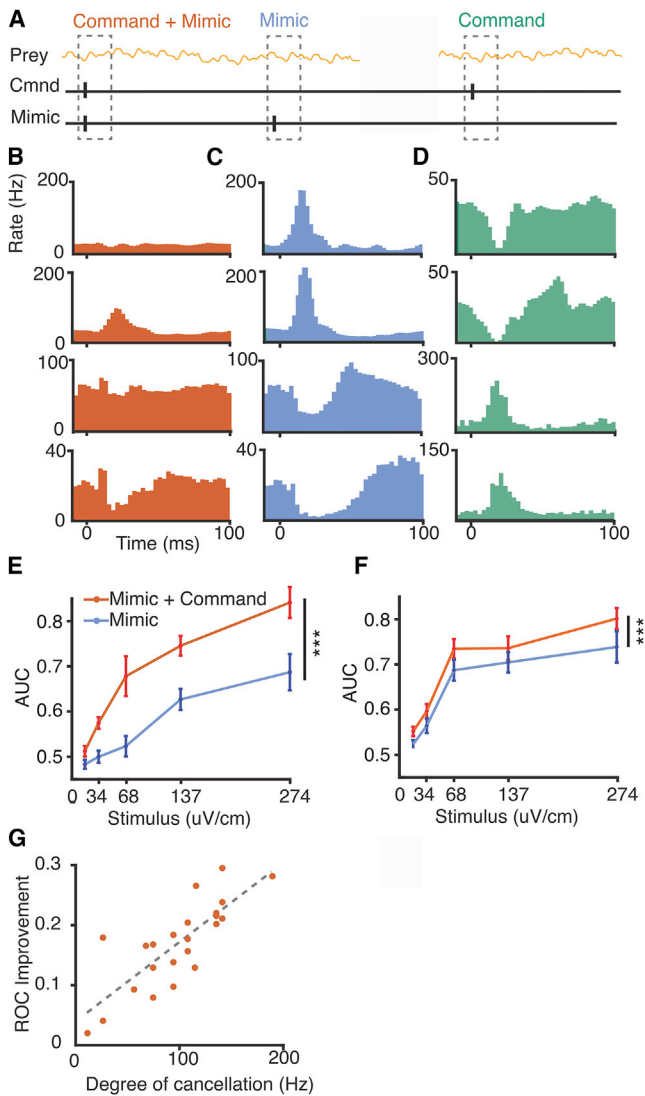


Figure 3. Improvements in Neural Detection of Prey-like Stimuli due to Negative Images

(A) Schematic of the experimental design. Neural detection of prey-like stimuli was quantified using ROC curves calculated for 100 ms periods following the EOD mimics paired with commands (red) as well as for interleaved mimics delivered independent of the command (cyan).

(B) Firing rate histograms triggered on the EOD command for two example E cells (top two rows) and two example I cells (bottom two rows).

(C) Histograms triggered on an identical EOD mimic delivered independent of the command in the same cells.

(D) Histograms triggered on the EOD command without an EOD mimic reveal negative images of the effects of the mimic in the same cells.

(E and F) Summary comparing detection performance for E cells ($n = 17$) (E) and I cells ($n = 31$) (F) in time windows following EOD mimics paired with the command (red) versus mimics delivered independent of the command (cyan). Mean AUC across stimulus intensities was greater when the mimic was paired with the command for both E and I cells, $p < 0.0001$ and $p < 0.0001$, respectively, one-tailed Wilcoxon signed rank test. Error bars indicate SEM.

(G) For E cells, improvements in AUC value for the paired versus independent condition is correlated on a cell-by-cell basis with the degree of cancellation of the EOD mimic in the paired condition, $R^2 = 0.57$.

that would normally evoke it, such that effects of the EOD on the neural detection of prey-like stimuli can be tested in the same cell with and without negative images. Responses to prey-like stimuli in E and I cells were measured while delivering EOD mimic pulses paired with the fish's spontaneously emitted EOD motor commands, similar to the experiments shown in Figure 2, but with the addition of interleaved EOD mimics delivered independent of the fish's commands (Figure 3A). EOD commands were paired with the mimic for at least 2 hr prior to recording to allow negative images to form. As expected based on past studies (Bell, 1981, 1982), E and I cell responses to EOD mimics paired with the command were reduced or, in some cases, completely cancelled (Figure 3B). In contrast, EOD mimics delivered independent of the command evoked strong responses (Figure 3C). Probing the response to the command alone revealed temporally-specific negative images of the effect of the EOD mimic (Figure 3D). Such negative images can account for the reduction of the response to EOD mimics paired with the command relative to those delivered independent of the command.

Prey-like stimulus detection performance was better in time windows following EOD mimics paired with commands compared to time windows following EOD mimics delivered independent of the command (Figures 3E and 3F). Since the only difference between the two conditions in this experiment is the timing of the EOD mimic relative to centrally originating electric organ corollary discharge signals, improvements in neural coding can be directly attributed to negative images. For E cells, the difference in detection performance in the two conditions (EOD mimics paired versus independent of the command) was correlated on a cell-by-cell basis with the extent to which responses to the EOD mimic were cancelled by the negative image (Figure 3G). No such correlation was observed for I cells, possibly due to the fact that EOD mimic sometimes drove the spike rate to zero. Since the magnitude of the response to the mimic cannot be determined in such cases, our estimate of the magnitude of cancellation is expected to be less accurate for I cells than for E cells.

A second approach takes advantage of our ability to rapidly induce negative image formation, such that the neural detection of prey-like stimuli can be tested in the same cell before, during, and after negative images have formed (Figure 4A). For these experiments, EOD mimics were delivered in the same spatial configuration as prey-like stimuli, i.e., locally within the receptive field of the recorded unit in contrast to the more spatially uniform EOD mimics used in Figures 2 and 3 (see STAR Methods). Such conditions mimic situations in which the spatial pattern of EOD-induced current flow through the skin changes, e.g., due to the location of the fish relative to large objects or non-conducting boundaries. In addition, characterizing detection performance in a situation in which the spatial characteristics of the EOD mimic and the prey-like stimulus match rules out a role for spatial filtering mechanisms in enhancing detection.

E and I cells exhibit stable responses with little or no response to the EOD command alone prior to pairing with an EOD mimic (Figures 4B and 4C, light green). Pairing an EOD mimic with the command resulted in strong initial firing rate modulations that diminished over 10–20 min or $\sim 2,500$ –5,000 commands

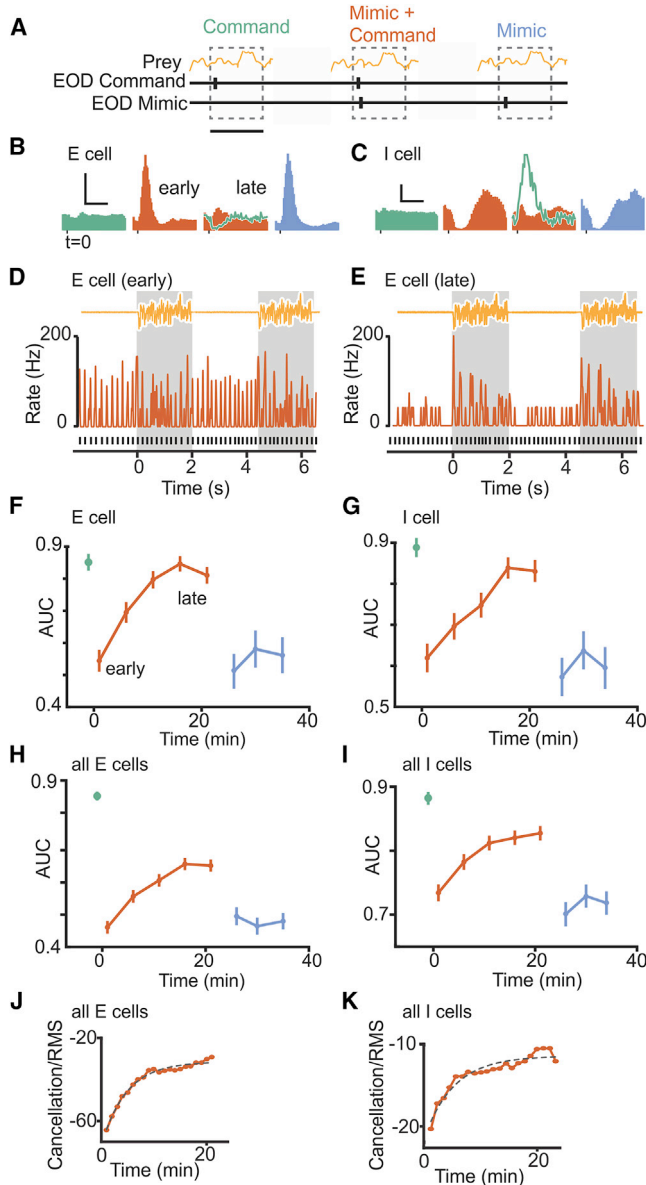


Figure 4. Time Course of Improvement in Neural Detection of Prey-like Stimuli due to Negative Images

(A) Schematic of the experimental design. Neural detection of prey-like stimuli was quantified using ROC curves calculated for baseline periods in which the fish issued EOD commands but no EOD mimics were delivered (green), pairing periods in which an EOD mimic was delivered following each command (red), and periods in which EOD mimics were delivered independent of the command (cyan). AUC was calculated over 100 ms windows following command or mimic onset. Scale bar, 100 ms.

(B and C) Firing rate histograms triggered on EOD command or mimic for example E (B) and I (C) cells. Note the reduction in the response to the EOD mimic during pairing (early versus late) due to the formation of a negative image (green line, late). Scale bars, 50 Hz, 50 ms in (B) and 30 Hz, 50 ms in (C).

(D and E) Smoothed firing rate early (D) versus late (E) in the pairing period for the E cell shown in (B). Black lines indicate time of EOD command, and yellow trace shows two prey-like stimulus presentations. Firing rate modulations evoked by the prey-like stimulus are masked by the effects of the EOD early during pairing but become evident late in pairing due to cancellation.

(Figures 4B and 4C, red, compare early and late). Turning the mimic off revealed a temporally-specific negative image of the response to the mimic during pairing (Figures 4B and 4C, dark green), consistent with previous studies. The larger negative images observed at the level of firing rates in I versus E cells is likely due to rectification, as such differences are not observed in intracellular recordings of the subthreshold membrane potential (Bell et al., 1997b; Mohr et al., 2003). Finally, delivering the same EOD mimic independent of the command evoked a strong response similar to that observed at the start of pairing (Figures 4B and 4C, cyan), consistent with the diminished response late in pairing being due to negative images rather than fatigue or peripheral adaptation. This pattern of results is consistent with previous studies (Bell, 1981, 1982).

The novelty of these experiments was to simultaneously deliver prey-like stimuli uncorrelated with the fish's EOD commands (Figures 4D and 4E), such that neural detection performance could be quantified before, during, and after negative image formation. Example E and I cells are shown in Figures 4F and 4G and averages across cells of each type are shown in Figures 4H and 4I. Prey detection performance was initially high in the absence of an EOD mimic (Figures 4F–4I, green) and dropped sharply when an EOD mimic was paired with the command (Figures 4F–4I, red). We observed a gradual increase in detection performance during pairing, consistent with a role for negative images in improving neural coding (Figures 4F–4I, early versus late). Finally, when we delivered the same EOD mimic but now independent of the EOD command, detection performance dropped once again (Figures 4F–4I, cyan). No gradual improvements in detection performance were observed in this condition, consistent with the observation that negative images only form when stimuli are time-locked to the fish's EOD command. The time course of improved prey detection performance during pairing matched the time course over which the effects of the EOD were cancelled in the same units (Figures 4J and 4K), again consistent with negative images improving neural coding of prey-like stimuli.

Though it is hypothesized that negative images perform a pure subtraction of the effects of the EOD, allowing ELL neurons to selectively encode behaviorally relevant stimuli, this has never

(F and G) Time course of neural detection performance quantified using ROC analysis for the same example E (F) and I (G) cells. Error bars are SEM calculated for repeated prey-like stimulus presentations.

(H) Averaged data for E cells ($n = 5$); error bars are the SEM across cells. Detection performance drops at the onset of pairing the command with an EOD mimic, $p < 0.0001$, and subsequently improves during pairing, $p < 0.0001$, multiple linear regression. For EOD mimics presented independent of the command, performance drops, $p < 0.0001$, but does not improve, $p = 0.83$, multiple linear regression.

(I) Averaged data for I cells ($n = 6$) as in (G). Detection performance drops at the onset of pairing, $p < 0.0001$, and subsequently improves, $p = 0.034$, multiple linear regression. For mimics presented independent of the command, performance drops, $p < 0.0001$, and does not improve, $p = 0.73$, multiple linear regression.

(J) Time course of cancellation of the effects of the EOD mimic during pairing for E cells as measured by the root-mean-square amplitude of the firing rate. Same data as in (H). Dashed line indicates exponential fit. Adjusted $R^2 = 0.98$. (K) Same display as (J) for I cells ($n = 6$). Adjusted $R^2 = 0.91$.

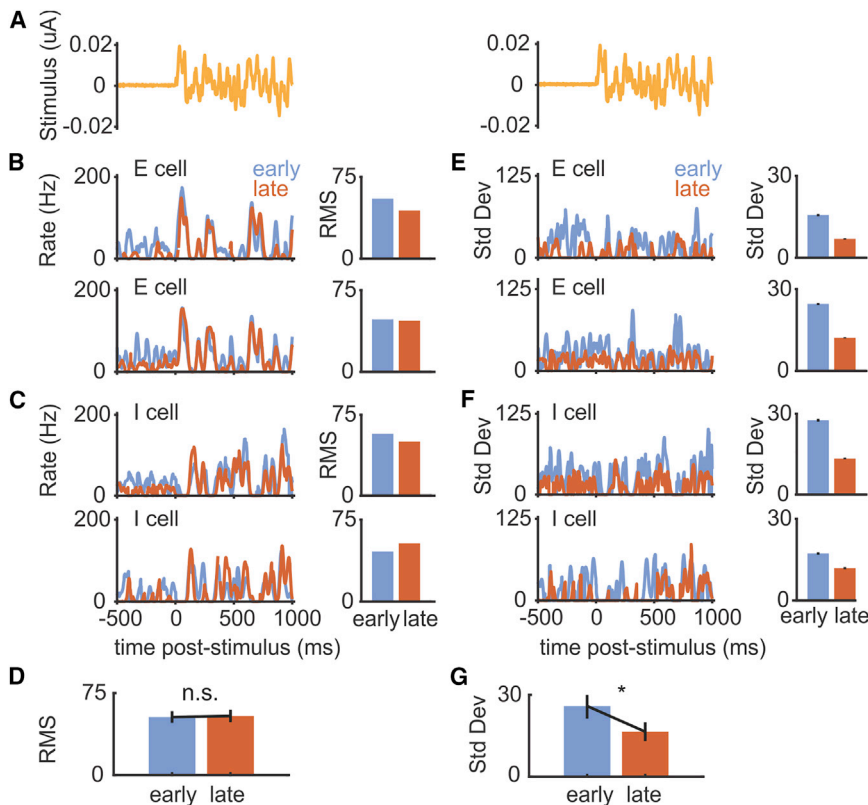


Figure 5. Cancellation Reduces the Variance of Responses to Prey-like Stimuli

(A) Prey-like stimulus waveform consisting of 2 s of frozen noise.

(B) Left: firing rate of two example E cells averaged over multiple presentations of a prey-like stimulus early (first 2 min) versus late (last 2 min) in the pairing period. Only periods 100 ms following the command are included in the averages. Right: RMS amplitude of the firing rate during the prey-like stimulus period for the same cells. RMS, root-mean-square.

(C) Same displays for two example I cells.

(D) RMS amplitude of prey-like stimulus responses is not different early versus late during pairing for all E and I cells shown in Figure 4 ($n = 11$, $p = 0.831$, two-tailed Wilcoxon signed rank test).

(E) Left: standard deviation of the firing rate of two example E cells over multiple presentations of a prey-like stimulus early versus late in the pairing period (same cells as in B). Right: standard deviation of the firing rate during the prey-like stimulus period for the same cells.

(F) Same displays for two example I cells (same cells as in C).

(G) Standard deviation of prey-like stimulus responses is reduced late versus early during pairing ($n = 11$, $p = 0.00195$, two-tailed Wilcoxon signed rank test).

Error bars indicate SEM.

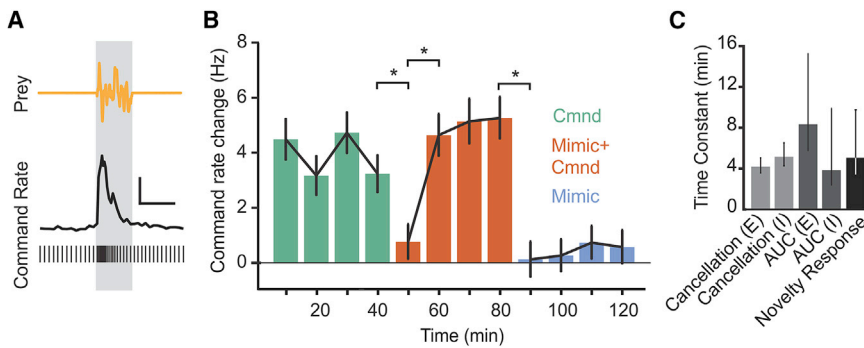
been directly tested. Alternatively, corollary discharge inputs could reduce neural sensitivity to sensory inputs during behavior (Bastian, 1986; Rotem et al., 2007; Schneider et al., 2014). We looked for evidence of a change in the sensitivity of principal cell responses to prey-like stimuli that could contribute to changes in detection performance. Inspection of the responses of the E and I cells used in Figure 4 revealed that firing rate modulations tracked the waveform of the prey-like stimulus with no changes in the root-mean-square amplitude of responses early versus late during pairing with an EOD mimic (Figures 5A–5D). Instead, we observed a clear reduction in the standard deviation of the response to prey-like stimuli late in pairing (Figures 5E–5G). Because the timing of the EOD mimics are controlled by the fish and are uncorrelated with the prey-like stimulus, strong responses evoked by the EOD mimic early in the pairing period contribute to the variance of the response to the prey-like stimulus. Hence, the reduction in the standard deviation of the response to prey-like stimuli late in the pairing period is consistent with the improvements in neural detection performance being due mainly or entirely to the subtraction of a negative image without any overall changes in sensitivity to the prey-like stimulus.

Enhanced Behavioral Responses to Prey-like Stimuli Associated with Negative Image Formation

Are the improvements in neural detection performance we observed accompanied by improvements at the behavioral level? To address this question, we took advantage of an electromotor behavior that can be readily measured in paralyzed fish

under the same experimental conditions as the neural recordings described above. The electromotor novelty response (NR) is a transient increase in the rate of the EOD command elicited by a sensory stimulus (Figure 6A). This behavior has been studied extensively in weakly electric fish and shares characteristics with orienting responses in other vertebrates (Hall et al., 1995; Post and von der Emde, 1999). As in past studies, we use it as a behavioral indication that the fish has detected an external stimulus (Hall et al., 1995).

We quantified the amplitude of NRs evoked by a prey-like stimulus. The experimental design, including both the prey-like stimulus and the EOD mimic amplitudes and spatial configurations were identical to those used for the neural recording experiments described in Figure 4. A baseline level of NRs was established by delivering prey-like stimuli in the absence of an EOD mimic (Figure 6B, green). Pairing a local EOD mimic with the command resulted in an initial drop in NR amplitude followed by a gradual return to baseline levels (Figure 6B, red), presumably due to the formation of negative images. When the EOD mimic was delivered independently of the EOD command, NR amplitudes again dropped but without a gradual return to baseline (Figure 6B, cyan). The lack of improvement in responses to prey-like stimuli in this condition is presumably because negative images cannot form (Bell, 1982). Hence, changes in behavioral detection of prey-like stimuli closely mirrored changes in neural detection performance measured under the same conditions. Moreover, cancellation of the effects of the EOD, improvements in neural detection performance quantified using ROC analysis, and improvements in behavioral detection performance



($n = 12$ repetitions of the experiment performed in 8 fish). Behavioral detection of prey-like stimuli, as measured by command rate changes, is stable during the first phase, $p = 0.31$, Friedman's non-parametric test; decreases on initial presentation of EOD mimic, $p = 0.0038$, Friedman's non-parametric test; and then improves during pairing, $p < 0.001$, Friedman's non-parametric test. Detection drops when the EOD mimic is delivered independent of command, $p < 0.001$, and does not improve, $p = 0.24$, Friedman's non-parametric test. Error bars indicate SEM.

(C) Time constants of cancellation of the effects of the EOD during pairing, improvements in neural detection or prey-like stimuli during pairing, and increases in behavioral responses to prey-like stimuli during pairing are similar. Error bars indicate 95% confidence intervals.

measured using the NR all exhibited a similar time course (Figure 6C). These results suggest that negative image formation not only improves the detection of prey-like stimuli at the level of neural coding in the ELL, but also enhances behavioral responses.

Manipulating Synaptic Plasticity in the ELL Disrupts Neural Coding and Behavioral Responses to Prey-like Stimuli

To provide a causal test of the hypothesis that negative images improve prey coding and detection, we attempted to block the associative synaptic plasticity underlying negative image formation. *In vitro* studies have demonstrated that anti-Hebbian synaptic plasticity in the ELL depends on N-methyl-D-aspartate (NMDA) receptors (Bell et al., 1997c; Han et al., 2000). Micropressure injections of the NMDA receptor antagonist 2-amino-5-phosphonopentanoic acid (AP5) into the VLZ molecular layer (Figure 7A) led to gradual changes in the responses of ELL principal cells to the EOD command. By 10–20 min after AP5 injections, both E and I cells exhibited increased firing with a prominent peak at a short delay (~15–20 ms) after the command and subsequent pairing with an EOD mimic failed to induce negative images (Figure 7B; Figure S4). Such large, sharply peaked command responses are never observed in the VLZ of naive fish and are opposite to what would be expected if AP5 acted mainly to block excitatory synaptic transmission. Moreover, E and I cell responses to the EOD mimic (delivered independently of the command) were unchanged in the presence of AP5 (Figure S4). In an additional set of experiments, we compared the effects of AP5 application on command responses and negative image formation with several agents reported to block long-term depression (LTD) in other systems and brain regions (Bear and Malenka, 1994; Jörntell and Hansel, 2006). We obtained preliminary data for an effect of the broad spectrum kinase inhibitor H7 and no effect of phosphatase inhibitors (Figure S5), suggesting a similarity with LTD in Purkinje cells and the gymnotid ELL (Belmeguenai and Hansel, 2005; Harvey-Girard et al., 2010; Harvey-Girard and Maler, 2013). However,

since the effects of H7 were not as large and consistent across cells as those of AP5 and since there is no *in vitro* data confirming the effects of H7 in the mormyrid ELL, we chose to use AP5 for further experiments.

The striking effect of AP5 injection provides a confirmation of models of negative image formation based on anti-Hebbian spike-timing-dependent plasticity at parallel fiber synapses. *In vitro* studies have shown that, although NMDA receptor antagonists block associative synaptic depression of parallel fiber synapses, non-associative potentiation of parallel fiber synapses remains intact (Bell et al., 1997c; Han et al., 2000). We used a computational model to understand the effects of blocking associative depression *in vivo*. The model is the same as that used in a previous study and consists of a single ELL principal cell that receives a large set of realistic granule cell corollary discharge responses generated based on past *in vivo* recordings (Kennedy et al., 2014). After each command, the strength of granule cell inputs are adjusted according to the measured anti-Hebbian spike-timing-dependent plasticity rule. To mimic the effects of AP5 injection, we set the magnitude of the associative depression component of the plasticity rule to zero while leaving the non-associative potentiation unchanged (Figure 7C, left). Without any additional tuning, the model principal cell exhibits a gradual increase in response at a short delay after the EOD command (Figure 7C, right), similar to the effects of AP5 injections on actual principal cell responses. With associative depression blocked, presynaptic action potentials driven by the EOD command lead to unchecked potentiation of granule cell synapses. The emergence of an early peak in the principal cell response can be explained by the observation from a past study that a large majority of granule cells fire at a short delay after the EOD motor command (Kennedy et al., 2014).

Next, we tested the effects of AP5 injection on responses to prey-like stimuli in ELL neurons. Gradual increases in responses to the EOD command following AP5 injection (Figure 7D; histograms represent pooled responses of E and I cells) were paralleled by a decline in neural detection performance (Figure 7E, left). A direct effect of AP5 on granule cells in these experiments

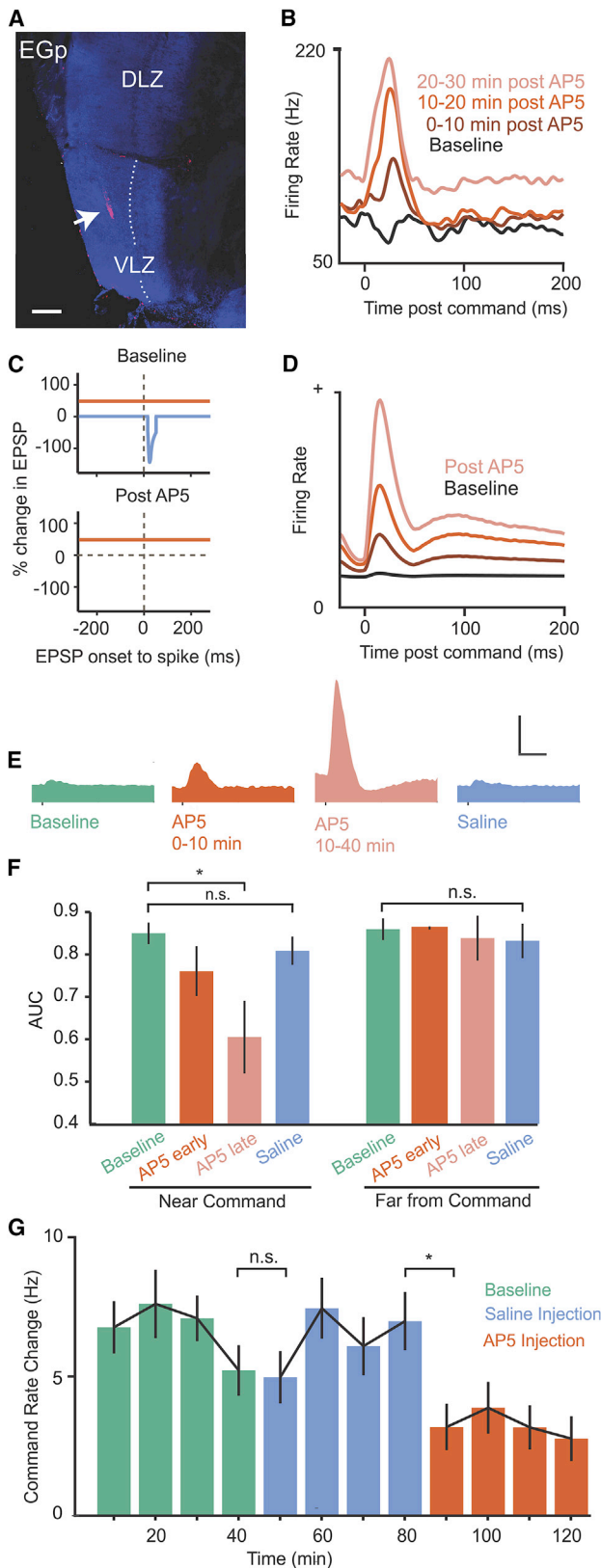


Figure 7. Manipulating Synaptic Plasticity in the ELL Disrupts Neural and Behavioral Detection of Prey-like Stimuli

(A) Fluorescent dextran (arrow) marks micropressure injection site of the NMDA receptor antagonist AP5 into the ELL molecular layer. Dotted line marks the boundary between the molecular and ganglion cell layers of VLZ. EGp, eminentia granularis posterior; VLZ, ventrolateral zone; DLZ, dorsolateral zone. Scale bar, 100 μ m.

(B) Smoothed firing rate triggered on the EOD command for an example E cell before and after an AP5 injection.

(C) Schematic of plasticity rule in ELL principal cells under normal conditions (top) and with NMDA receptors blocked (bottom).

(D) Changes in EOD command responses in a model ELL principal cell induced by setting the rate of associative synaptic depression to zero (compare with B).

(E) Average command responses of ELL principal cells before AP5 injection (n = 40, green), 0-10 min after injection (n = 3, red), 10-40 min after injection (n = 11, light red), and following saline injections (n = 22, blue). Scale bar, 100 Hz, 50 ms.

(F) Left: prey-like stimulus detection quantified in 100 ms windows triggered on the EOD command before (green), 0-10 min after (dark red), and 10-40 min after (light red) AP5 injection and following saline injection (blue). Same data as in (E). AP5 injection resulted in a significant decrease in detection performance at 10-40 min, $p < 0.0001$, one-tailed Wilcoxon rank-sum test. No significant changes in detection performance were observed after saline injections or when detection performance was quantified late in the command cycle when effects of AP5 on firing rate were minimal (right: 100 ms analysis window beginning 100 ms after the command).

(G) Command rate changes evoked by a prey-like stimulus during a baseline condition (green) and following micropressure injections of saline (blue) or AP5 (red) into the ELL molecular layer. AP5 injections reduced command rate changes evoked by a prey-like stimulus, $p < 0.0001$, whereas saline injections had no effect ($p = 0.97$, Friedman's non-parametric test, n = 6 repetitions of the experiment in 6 fish).

Error bars in (F) and (G) indicate SEM.

is unlikely because of their remote location in an external granule cell mass overlying the ELL molecular layer (Figure 7A). To rule out the possibility that NMDA receptor blockade interferes with electrosensory encoding in the ELL independent of its effects on synaptic plasticity (Marcoux et al., 2016), we analyzed prey-like stimulus detection performance in time windows far from the EOD command. Detection performance was unaffected away from the command (Figure 7E, right), consistent with effects of AP5 being exerted mainly or entirely through the elevated firing induced by non-associative potentiation of corollary discharge inputs.

Finally, we measured behavioral NRs induced by prey-like stimuli before and after AP5 injections. NRs were evoked by prey-like stimuli delivered to a spatially restricted region of the skin, as in the experiments shown in Figure 6. Micropressure injections of AP5 were made into the VLZ molecular layer, targeting a somatotopic location corresponding to the location of the prey-like stimulus delivered to electroreceptors on the skin. AP5 injections strongly reduced the amplitude of NRs evoked by prey-like stimuli relative to baseline conditions, whereas saline injections had no effect (Figure 7F). Additional experiments showed similar reductions in NRs when AP5 injections were performed immediately after the baseline period (Figure S6). Agents that block non-associative potentiation in the ELL have yet to be identified (Han et al., 2000). Hence, we were not able to directly test the effects of blocking negative image formation on neural or behavioral detection performance. Nevertheless, the results described above indicate the potential

for synaptic plasticity to powerfully shape the output of the ELL and affect behavior.

DISCUSSION

Extensive past studies of cerebellum-like structures at the first stage of electrosensory processing in fish (Bastian, 1996; Bell et al., 1997a, 2008; Bodznick et al., 1999; Harvey-Girard et al., 2010; Bol et al., 2011; Marsat and Maler, 2012; Harvey-Girard and Maler, 2013) and a more recent study of a cerebellum-like structure at the first stage of auditory processing in mice (Singla et al., 2017) suggest that the subtraction of internally generated predictions of the sensory consequences of behavior enhances the detection and processing of external sensory stimuli. The present study provides both neurophysiological and behavioral evidence supporting this hypothesis. We showed that the formation of negative image of the predictable electrosensory consequences of the fish's own EOD was accompanied by improvements in the neural coding of external, prey-like stimuli in ELL principal cells. Importantly, the improvements could not be accounted for by other processes, such as spatial filtering or gain changes. Such improvements were also observed under several different experimental conditions (e.g., different relative strengths of external versus self-generated sensory inputs) intended to represent a range of behaviorally relevant conditions. An additional set of experiments demonstrated an enhancement of behavioral responses to prey-like stimuli that paralleled negative image formation. Finally, disrupting synaptic plasticity in the ELL interfered with both neural coding and behavioral responses to prey-like stimuli. Together with past studies, these results provide an integrated account—spanning levels of synapses, circuits, sensory coding, and behavior—of how combining external sensory input with internally generated prediction enhances sensory processing.

Although it has long been hypothesized that cancelling self-generated inputs via the generation of negative images could enhance sensory processing (Sperry, 1950; von Holst and Mittelstaedt, 1950) (Figure 1), there are a number of reasons why implementing such a scheme in neural circuits could be problematic. First, while such models assume linear operations, actual neurons, including those in the ELL, are non-linear in numerous respects (Gabbiani et al., 1996; Koch and Segev, 2000). Cancellation in principal cells is hypothesized to be due to the linear summation of electrosensory input onto basilar dendrites and corollary discharge input onto apical dendrites. Such linear summation is desirable because it would allow negative images to cancel the effects of the EOD without altering the manner in which they encode behaviorally relevant sensory inputs. However, studies of the ELL in weakly electric gymnotid fish have shown that lesions or inactivation of the granule cells dramatically increase the gain of responses to electrosensory stimuli in principal cells (Bastian, 1986). Studies of gymnotid ELL have also demonstrated that non-linear, burst firing mechanisms are critical for encoding prey-like stimuli (Chacron et al., 2003; Gabbiani et al., 1996; Metzner et al., 1998; Oswald et al., 2004) and that the dynamics of burst firing can be altered by dendritic inputs (Chacron et al., 2005; Mehaffey et al., 2007; Turner et al., 2002). Principal cells in the mormyrid ELL also exhibit burst

firing (Sugawara et al., 1999), raising the possibility that the negative image—a large dendritic input—might interfere with burst dynamics and the coding of prey-like stimuli. Nevertheless, our results show that negative images improve neural detection performance (Figures 3 and 4) without grossly altering responses to prey-like stimuli (Figure 5). Hence, our findings are consistent with the notion that negative images perform a pure subtraction of the effects of the effects of the EOD. How linear behavior arises out of interactions between nonlinear components is an important general question in neuroscience that may be illuminated by further studies of the ELL.

Variability or noise is an additional key consideration for any scheme relying on the subtraction of two large signals. ELL neuron responses to prey-like stimuli are expected to be subject to noise (for example, associated with synaptic transmission) proportional to the sum of the variance of the negative image and the variance of the response to the EOD. Noise due to the subtraction of these two large signals might be expected to overwhelm responses to prey. Results of the present study indicate that this is not the case, as demonstrated, for example, by the observation that negative images enhance neural detection performance across a range of prey-like stimulus amplitudes (Figure 3). Whether the ELL employs specific mechanisms for reducing noise is another topic for future studies. Revising existing models of the ELL to incorporate realistic assumptions regarding nonlinearities in the system and estimates of noise constrained by the data will further strengthen our understanding of how synaptic plasticity operating within the well-defined circuitry of the ELL shapes adaptive neural processing and behavior. Failure of more realistic models to match the data will motivate studies of additional aspects of ELL circuitry that are not well understood. For example, current models largely ignore the role of inhibition and do not distinguish between two distinct classes of ELL neurons—the glutamatergic efferent cells studied here versus the GABAergic medium ganglion (MG) cells. Both classes integrate peripheral electrosensory input and plastic corollary discharge signals (Bell et al., 1997b). MG cells inhibit efferent cells and share numerous similarities with cerebellar Purkinje cells (Bell et al., 2008).

The dramatic effects of blocking NMDA receptors in the ELL provide strong support for existing models of negative image formation based on anti-Hebbian spike-timing-dependent plasticity (Kennedy et al., 2014; Roberts and Bell, 2000). Such models predict that with NMDA-receptor-dependent associative synaptic depression blocked, non-associative potentiation will proceed unchecked and the response of an ELL principal cell to the EOD command will reflect the sum of its granule cell inputs. The temporal profile of ELL principal cell responses after NMDA receptor blockade closely resembled the summed granule cell corollary discharge response as determined by recordings from a large number of granule cells in a previous study (Kennedy et al., 2014). Regarding the cellular mechanisms for synaptic plasticity in the mormyrid ELL, several comparisons to other systems can be drawn based on previous studies and our present results. The NMDA receptor dependence of associative depression in the mormyrid ELL is shared by some forms of LTD in the neocortex, hippocampus, dorsal cochlear nucleus, gymnotid ELL, and cerebellum (Bear and Malenka, 1994; Jörntell

and Hansel, 2006; Tzounopoulos et al., 2007; Harvey-Girard et al., 2010; Harvey-Girard and Maler, 2013). However, unlike at mature parallel fiber-Purkinje cell synapses, transmission at parallel fiber synapse-principal cell synapses in the ELL exhibits a prominent NMDA-receptor-mediated component (Berman and Maler, 1998; Grant et al., 1998). Moreover, the NMDA receptor dependence of LTD in Purkinje cells is due to NMDA-receptor-mediated calcium influx at climbing fiber synapses rather than at parallel fiber synapses (Piochon et al., 2010). Preliminary evidence from *in vivo* drug applications in the present study (Figure S5) suggests that kinase inhibitors may be necessary for associative depression in the mormyrid ELL. This requires verification *in vitro*. However, if correct, it would indicate an additional similarity between plasticity in cerebellum-like structures (including the ELL of both mormyrid and gymnotid fish) and the cerebellum (Belmeguenai and Hansel, 2005; Harvey-Girard et al., 2010; Harvey-Girard and Maler, 2013). In contrast, NMDA-receptor-dependent LTD depends on phosphatases in the neocortex and hippocampus (Bear and Malenka, 1994). More broadly, these observations are interesting in light of the evidence that dysregulation of synaptic plasticity may play a role in neurological disorders ranging from autism to tinnitus (Auerbach et al., 2011; Bear et al., 2004; Shore et al., 2016). Our results provide a clear case in which dysregulation of synaptic plasticity leads to aberrant circuit output and disruptions of sensory processing and behavior.

STAR★METHODS

Detailed methods are provided in the online version of this paper and include the following:

- KEY RESOURCES TABLE
- CONTACT FOR REAGENT AND RESOURCE SHARING
- EXPERIMENTAL MODEL AND SUBJECT DETAILS
- METHOD DETAILS
 - Surgery
 - Electrophysiology
 - EOD Mimics
 - Prey-like Stimuli
 - AP5 Injections
 - Novelty Response Experiments
 - Modeling
 - Histology
- QUANTIFICATION AND STATISTICAL ANALYSIS
 - Analysis of Spike Train Data
 - ROC Analysis
 - Novelty Response Analysis
- DATA AND SOFTWARE AVAILABILITY

SUPPLEMENTAL INFORMATION

Supplemental Information includes six figures and can be found with this article online at <https://doi.org/10.1016/j.neuron.2018.06.006>.

ACKNOWLEDGMENTS

This work was supported by grants from the NSF (1025849) to N.B.S. and L.F.A. and the NIH (NS075023) to N.B.S. and by the Irma T. Hirschl Trust.

L.F.A. was further supported by the Simons and Swartz Foundations and by NSF NeuroNex Award DBI-1707398. Thanks to C. Dempsey and S.Z. Muller for assistance with modeling and E. Batty for assistance with behavioral experiments.

AUTHOR CONTRIBUTIONS

A.G.E. and N.B.S. performed the experiments and analyzed data. N.B.S. and L.F.A. conceived of the project. N.B.S., L.F.A., and A.G.E. designed the experiments and wrote the manuscript.

DECLARATION OF INTERESTS

The authors declare no competing interests.

Received: February 5, 2018

Revised: May 3, 2018

Accepted: June 4, 2018

Published: July 11, 2018

REFERENCES

- Auerbach, B.D., Osterweil, E.K., and Bear, M.F. (2011). Mutations causing syndromic autism define an axis of synaptic pathophysiology. *Nature* 480, 63–68.
- Bastian, J. (1986). Gain control in the electrosensory system mediated by descending inputs to the electrosensory lateral line lobe. *J. Neurosci.* 6, 553–562.
- Bastian, J. (1993). The role of amino acid neurotransmitters in the descending control of electroreception. *J. Comp. Physiol. A Neuroethol. Sens. Neural Behav. Physiol.* 172, 409–423.
- Bastian, J. (1996). Plasticity in an electrosensory system. I. General features of a dynamic sensory filter. *J. Neurophysiol.* 76, 2483–2496.
- Bear, M.F., and Malenka, R.C. (1994). Synaptic plasticity: LTP and LTD. *Curr. Opin. Neurobiol.* 4, 389–399.
- Bear, M.F., Huber, K.M., and Warren, S.T. (2004). The mGluR theory of fragile X mental retardation. *Trends Neurosci.* 27, 370–377.
- Bell, C.C. (1981). An efference copy which is modified by reafferent input. *Science* 214, 450–453.
- Bell, C.C. (1982). Properties of a modifiable efference copy in an electric fish. *J. Neurophysiol.* 47, 1043–1056.
- Bell, C.C. (2001). Memory-based expectations in electrosensory systems. *Curr. Opin. Neurobiol.* 11, 481–487.
- Bell, C.C., and Russell, C.J. (1978). Effect of electric organ discharge on ampullary receptors in a mormyrid. *Brain Res.* 145, 85–96.
- Bell, C.C., and Szabo, T. (1986). Electroreception in mormyrid fish: central anatomy. In *Electroreception*, T.H. Bullock and W. Heiligenberg, eds. (John Wiley & Sons), pp. 375–421.
- Bell, C.C., Grant, K., and Serrier, J. (1992). Sensory processing and corollary discharge effects in the mormyromast regions of the mormyrid electrosensory lobe. I. Field potentials, cellular activity in associated structures. *J. Neurophysiol.* 68, 843–858.
- Bell, C., Bodznick, D., Montgomery, J., and Bastian, J. (1997a). The generation and subtraction of sensory expectations within cerebellum-like structures. *Brain Behav. Evol.* 50 (Suppl 1), 17–31.
- Bell, C.C., Caputi, A., and Grant, K. (1997b). Physiology and plasticity of morphologically identified cells in the mormyrid electrosensory lobe. *J. Neurosci.* 17, 6409–6423.
- Bell, C.C., Han, V.Z., Sugawara, Y., and Grant, K. (1997c). Synaptic plasticity in a cerebellum-like structure depends on temporal order. *Nature* 387, 278–281.
- Bell, C.C., Han, V., and Sawtell, N.B. (2008). Cerebellum-like structures and their implications for cerebellar function. *Annu. Rev. Neurosci.* 31, 1–24.
- Belmeguenai, A., and Hansel, C. (2005). A role for protein phosphatases 1, 2A, and 2B in cerebellar long-term potentiation. *J. Neurosci.* 25, 10768–10772.

- Berman, N.J., and Maler, L. (1998). Distal versus proximal inhibitory shaping of feedback excitation in the electrosensory lateral line lobe: implications for sensory filtering. *J. Neurophysiol.* *80*, 3214–3232.
- Bodznick, D., and Montgomery, J.C. (1992). Suppression of ventilatory reafference in the elasmobranch electrosensory system: medullary neuron receptive fields support a common mode rejection mechanism. *J. Exp. Biol.* *171*, 127–137.
- Bodznick, D., and Montgomery, J.C. (2005). The physiology of low-frequency electrosensory systems. In *Electroreception*, T.H. Bullock, C.D. Hopkins, A.N. Popper, and R.R. Fay, eds. (Springer), pp. 132–153.
- Bodznick, D., Montgomery, J.C., and Carey, M. (1999). Adaptive mechanisms in the elasmobranch hindbrain. *J. Exp. Biol.* *202*, 1357–1364.
- Bol, K., Marsat, G., Harvey-Girard, E., Longtin, A., and Maler, L. (2011). Frequency-tuned cerebellar channels and burst-induced LTD lead to the cancellation of redundant sensory inputs. *J. Neurosci.* *31*, 11028–11038.
- Brooks, J.X., Carriot, J., and Cullen, K.E. (2015). Learning to expect the unexpected: rapid updating in primate cerebellum during voluntary self-motion. *Nat. Neurosci.* *18*, 1310–1317.
- Chacron, M.J., Doiron, B., Maler, L., Longtin, A., and Bastian, J. (2003). Non-classical receptive field mediates switch in a sensory neuron's frequency tuning. *Nature* *423*, 77–81.
- Chacron, M.J., Maler, L., and Bastian, J. (2005). Feedback and feedforward control of frequency tuning to naturalistic stimuli. *J. Neurosci.* *25*, 5521–5532.
- Dayan, P., and Abbott, L.F. (2001). *Theoretical Neuroscience: Computational and Mathematical Modeling of Neural Systems* (MIT Press).
- Doiron, B., Chacron, M.J., Maler, L., Longtin, A., and Bastian, J. (2003). Inhibitory feedback required for network oscillatory responses to communication but not prey stimuli. *Nature* *421*, 539–543.
- Engelmann, J., Gertz, S., Goulet, J., Schuh, A., and von der Emde, G. (2010). Coding of stimuli by ampullary afferents in *Gnathonemus petersii*. *J. Neurophysiol.* *104*, 1955–1968.
- Gabbiani, F., Metzner, W., Wessel, R., and Koch, C. (1996). From stimulus encoding to feature extraction in weakly electric fish. *Nature* *384*, 564–567.
- Grant, K., Sugawara, Y., Gómez, L., Han, V.Z., and Bell, C.C. (1998). The mormyrid electrosensory lobe *in vitro*: physiology and pharmacology of cells and circuits. *J. Neurosci.* *18*, 6009–6025.
- Grüsser, O.J. (1986). Interaction of efferent and afferent signals in visual perception. A history of ideas and experimental paradigms. *Acta Psychol. (Amst.)* *63*, 3–21.
- Hall, J.C., Bell, C., and Zelick, R. (1995). Behavioral evidence of a latency code for stimulus intensity in mormyrid electric fish. *J. Comp. Physiol. A Neuroethol. Sens. Neural Behav. Physiol.* *177*, 29–39.
- Han, V.Z., Bell, C.C., Grant, G., and Sugawara, Y. (1999). Mormyrid electrosensory lobe *in vitro*: morphology of cells and circuits. *J. Comp. Neurol.* *404*, 359–374.
- Han, V.Z., Grant, K., and Bell, C.C. (2000). Reversible associative depression and nonassociative potentiation at a parallel fiber synapse. *Neuron* *27*, 611–622.
- Harvey-Girard, E., and Maler, L. (2013). Dendritic SK channels convert NMDA-R-dependent LTD to burst timing-dependent plasticity. *J. Neurophysiol.* *110*, 2689–2703.
- Harvey-Girard, E., Lewis, J., and Maler, L. (2010). Burst-induced anti-Hebbian depression acts through short-term synaptic dynamics to cancel redundant sensory signals. *J. Neurosci.* *30*, 6152–6169.
- Jörntell, H., and Hansel, C. (2006). Synaptic memories upside down: bidirectional plasticity at cerebellar parallel fiber-Purkinje cell synapses. *Neuron* *52*, 227–238.
- Kennedy, A., Wayne, G., Kaifosh, P., Alviña, K., Abbott, L.F., and Sawtell, N.B. (2014). A temporal basis for predicting the sensory consequences of motor commands in an electric fish. *Nat. Neurosci.* *17*, 416–422.
- Kim, A.J., Fitzgerald, J.K., and Maimon, G. (2015). Cellular evidence for efference copy in *Drosophila* visuomotor processing. *Nat. Neurosci.* *18*, 1247–1255.
- Koch, C., and Segev, I. (2000). The role of single neurons in information processing. *Nat. Neurosci.* *3 (Suppl)*, 1171–1177.
- Krasne, F.B., and Bryan, J.S. (1973). Habituation: regulation through presynaptic inhibition. *Science* *182*, 590–592.
- Leinweber, M., Ward, D.R., Sobczak, J.M., Attinger, A., and Keller, G.B. (2017). A sensorimotor circuit in mouse cortex for visual flow predictions. *Neuron* *95*, 1420–1432.e5.
- Malpeli, J.G., and Schiller, P.H. (1979). A method of reversible inactivation of small regions of brain tissue. *J. Neurosci. Methods* *1*, 143–151.
- Marcoux, C.M., Clarke, S.E., Nesse, W.H., Longtin, A., and Maler, L. (2016). Balanced ionotropic receptor dynamics support signal estimation via voltage-dependent membrane noise. *J. Neurophysiol.* *115*, 530–545.
- Marsat, G., and Maler, L. (2012). Preparing for the unpredictable: adaptive feedback enhances the response to unexpected communication signals. *J. Neurophysiol.* *107*, 1241–1246.
- Mehaffey, W.H., Fernandez, F.R., Maler, L., and Turner, R.W. (2007). Regulation of burst dynamics improves differential encoding of stimulus frequency by spike train segregation. *J. Neurophysiol.* *98*, 939–951.
- Metzner, W., Koch, C., Wessel, R., and Gabbiani, F. (1998). Feature extraction by burst-like spike patterns in multiple sensory maps. *J. Neurosci.* *18*, 2283–2300.
- Mohr, C., Roberts, P.D., and Bell, C.C. (2003). The mormyromast region of the mormyrid electrosensory lobe. I. Responses to corollary discharge and electrosensory stimuli. *J. Neurophysiol.* *90*, 1193–1210.
- Montgomery, J.C. (1984). Noise cancellation in the electrosensory system of the thornback ray; common mode rejection of input produced by the animal's own ventilatory movement. *J. Comp. Physiol. A Neuroethol. Sens. Neural Behav. Physiol.* *155*, 103–111.
- Montgomery, J.C., and Bodznick, D. (1993). Hindbrain circuitry mediating common mode suppression of ventilatory reafference in the electrosensory system of the little skate *Raja erinacea*. *J. Exp. Biol.* *183*, 203–215.
- Oswald, A.M., Chacron, M.J., Doiron, B., Bastian, J., and Maler, L. (2004). Parallel processing of sensory input by bursts and isolated spikes. *J. Neurosci.* *24*, 4351–4362.
- Piochon, C., Levenes, C., Ohtsuki, G., and Hansel, C. (2010). Purkinje cell NMDA receptors assume a key role in synaptic gain control in the mature cerebellum. *J. Neurosci.* *30*, 15330–15335.
- Post, N., and von der Emde, G. (1999). The “novelty response” in an electric fish: response properties and habituation. *Physiol. Behav.* *68*, 115–128.
- Poulet, J.F., and Hedwig, B. (2007). New insights into corollary discharges mediated by identified neural pathways. *Trends Neurosci.* *30*, 14–21.
- Requarth, T., and Sawtell, N.B. (2014). Plastic corollary discharge predicts sensory consequences of movements in a cerebellum-like circuit. *Neuron* *82*, 896–907.
- Richmond, B.J., and Wurtz, R.H. (1980). Vision during saccadic eye movements. II. A corollary discharge to monkey superior colliculus. *J. Neurophysiol.* *43*, 1156–1167.
- Roberts, P.D., and Bell, C.C. (2000). Computational consequences of temporally asymmetric learning rules: II. Sensory image cancellation. *J. Comput. Neurosci.* *9*, 67–83.
- Roberts, B.L., and Russell, I.J. (1972). The activity of lateral-line efferent neurons in stationary and swimming dogfish. *J. Exp. Biol.* *57*, 435–448.
- Rotem, N., Sestieri, E., Cohen, D., Paulin, M., Meiri, H., and Yarom, Y. (2007). The functional architecture of the shark's dorsal-octavolateral nucleus: an *in vitro* study. *J. Exp. Biol.* *210*, 2730–2742.
- Schneider, D.M., Nelson, A., and Mooney, R. (2014). A synaptic and circuit basis for corollary discharge in the auditory cortex. *Nature* *513*, 189–194.
- Shore, S.E., Roberts, L.E., and Langguth, B. (2016). Maladaptive plasticity in tinnitus—triggers, mechanisms and treatment. *Nat. Rev. Neurol.* *12*, 150–160.

- Singla, S., Dempsey, C., Warren, R., Enikolopov, A.G., and Sawtell, N.B. (2017). A cerebellum-like circuit in the auditory system cancels responses to self-generated sounds. *Nat. Neurosci.* *20*, 943–950.
- Sperry, R.W. (1950). Neural basis of the spontaneous optokinetic response produced by visual inversion. *J. Comp. Physiol. Psychol.* *43*, 482–489.
- Sugawara, Y., Grant, K., Han, V., and Bell, C.C. (1999). Physiology of electro-sensory lateral line lobe neurons in *Gnathonemus petersii*. *J. Exp. Biol.* *202*, 1301–1309.
- Turner, R.W., Lemon, N., Doiron, B., Rashid, A.J., Morales, E., Longtin, A., Maler, L., and Dunn, R.J. (2002). Oscillatory burst discharge generated through conditional backpropagation of dendritic spikes. *J. Physiol. Paris* *96*, 517–530.
- Tzounopoulos, T., Rubio, M.E., Keen, J.E., and Trussell, L.O. (2007). Coactivation of pre- and postsynaptic signaling mechanisms determines cell-specific spike-timing-dependent plasticity. *Neuron* *54*, 291–301.
- von der Emde, G., and Bleckmann, H. (1998). Finding food: senses involved in foraging for insect larvae in the electric fish *gnathonemus petersii*. *J. Exp. Biol.* *201*, 969–980.
- von Holst, E. (1954). Relations between the central nervous system and the peripheral organs. *Br. J. Anim. Behav.* *2*, 89–94.
- von Holst, E., and Mittelstaedt, H. (1950). The reafference principle. *Naturwissenschaften* *37*, 464–476.
- Wilkens, L.A., and Hofmann, M.H. (2005). Behavior of animals with passive, low-frequency electrosensory systems. In *Electroreception*, T.H. Bullock, C.D. Hopkins, A.N. Popper, and R.R. Fay, eds. (Springer), pp. 229–263.
- Zipser, B., and Bennett, M.V.L. (1976). Interaction of electrosensory and electromotor signals in lateral line lobe of a mormyrid fish. *J. Neurophysiol.* *39*, 713–721.

STAR★METHODS

KEY RESOURCES TABLE

| REAGENT or RESOURCE | SOURCE | IDENTIFIER |
|---|--------|-------------|
| Chemicals, Peptides, and Recombinant Proteins | | |
| H7-dihydrochloride | Tocris | 108930-17-2 |
| D-AP5 | Tocris | 79055-68-8 |
| FK-506 | Tocris | 104987-11-3 |
| Okadaic acid | Tocris | 78111-17-8 |

CONTACT FOR REAGENT AND RESOURCE SHARING

Further information and requests for resources and reagents should be directed to and will be fulfilled by the Lead Contact Nathaniel Sawtell (ns2635@columbia.edu).

EXPERIMENTAL MODEL AND SUBJECT DETAILS

Male and female Mormyrid fish (7–12 cm in length) of the species *Gnathonemus petersii* were used in these experiments. Fish were housed in 60 gallon tanks in groups of 5–20. Water conductivity was maintained between 40–65 microsiemens, both in the fish's home tanks and during experiments. All experiments performed in this study adhere to the American Physiological Society's *Guiding Principles in the Care and Use of Animals* and were approved by the Institutional Animal Care and Use Committee of Columbia University.

METHOD DETAILS

Surgery

Fish were anesthetized (MS:222, 1:25,000) and held against a foam pad. Skin on the dorsal surface of the head was removed and a long-lasting local anesthetic (0.75% Bupivacaine) was applied to the wound margins. A plastic rod was cemented to the anterior portion of the skull to hold the head rigid. The posterior portion of the skull overlying ELL was removed. In a subset of experiments the valvula cerebelli was reflected laterally allowing direct visualization of the molecular layer of the caudal lobe of the cerebellum and the eminentia granularis posterior (EGp). Gallamine triethiodide (Flaxedil) was given at the end of the surgery (~20 $\mu\text{g}/\text{cm}$ of body length) and the anesthetic was removed. Aerated water was passed over the fish's gills for respiration. Paralysis blocks the effect of electromotoneurons on the electric organ, preventing the EOD, but the motor command signal that would normally elicit an EOD continues to be emitted by the electromotoneurons at a variable rate of 2 to 5 Hz. The timing of the EOD motor command can be measured precisely (see below) and the central effects of electric organ corollary discharge inputs can be observed in isolation from the electrosensory input that would normally result from the EOD.

Electrophysiology

Extracellular single-unit recordings were made using glass microelectrodes (2–10 M Ω) filled with 2M NaCl, as described previously (Bell, 1982; Requarth and Sawtell, 2014). Recording locations within the VLZ were first established using characteristic field potentials evoked by the EOD command (Bell et al., 1992). The precise location of the recording pipette with respect to the VLZ somatotopic map was subsequently determined by finding the skin region for which low-frequency electrosensory stimulation delivered via a dipole electrode evoked multi-unit responses. Ampullary electroreceptor afferents, E cells and I cells are located in different layers of ELL and have distinctive electrophysiological characteristics (Bell, 1982; Bell and Szabo, 1986). Ampullary afferents terminate in the deep layers of ELL, exhibit highly regular spontaneous firing at around 50 Hz, and increase firing rate in response to an electrosensory stimulus that makes the pore of the receptor positive with respect to the basal face within the body (Bell and Russell, 1978; Engelmann et al., 2010). E cells are located in the plexiform layer and I cell in the ganglion layer. E and I cells both fire much more irregularly and at lower rates than afferents (Bell, 1982). E cells are excited by the same stimulus polarity as afferents while I cells are excited by the opposite polarity. Cross-correlation analysis confirmed that units identified as E and I cells are non-overlapping groups with respect to their responses to low-frequency electrosensory stimuli (Figure S1). Previous studies using intracellular recording and biocytin labeling and antidromic stimulation from the midbrain have shown that E and I cells correspond to two morphologically distinct types of ELL efferent cells known as large fusiform and large ganglion cells (Bell et al., 1997b). In addition to efferent cells, the other major large cells of ELL are the medium ganglion cells (Bell et al., 1997b; Grant et al., 1998; Han et al., 1999). Recordings

were occasionally obtained from medium ganglion cells identified, as in previous studies, by the presence of two distinct spike types (Bell et al., 1997b; Grant et al., 1998). Such recordings were not included in the present analysis.

EOD Mimics

The EOD motor command signal was recorded with a Ag-AgCl electrode placed over the electric organ. The command signal is the synchronized volley of electromotoneurons that would normally elicit an EOD in the absence of neuromuscular blockade. The command signal lasts about 3 ms and consists of a small negative wave followed by three larger biphasic waves. Onset of EOD command was recorded as the negative peak of the first large biphasic wave in the command signal. When locked to the electric organ motor command, the EOD mimic was presented 4.5ms following this time. For Figures 2 and 3 the EOD mimic was a 200 μ s duration square pulse delivered between an electrode in the stomach and another positioned near the electric organ in the tail. The amplitude was 200 μ A at the output of the stimulus isolation unit for Figure 2 and 30-50 μ A for Figure 3. For both experiments the electrode in the stomach was negative. A previous study has shown that the effects of such pulses on ampullary afferent firing are similar to those of the fish's natural EOD (Bell and Russell, 1978). Past studies of the natural EOD in non-paralyzed mormyrid fish show that its effects on passive electroreceptors vary in magnitude depending on water conductivity (Bell and Russell, 1978), which is subject to large variation in the natural habitat of mormyrids (e.g., due to rainfall and seasonal flooding). The spatial pattern of activation due to the EOD may also vary, for example depending on the location of the fish relative to large objects or non-conducting boundaries or due to physical damage to the skin. For these reasons, the amplitude and spatial patterns of EOD mimics were varied in our experiments (see STAR Methods). The amplitude of the EOD mimic used in Figure 2 was chosen to evoke firing rate modulations in ampullary afferents at the top of the range reported previously for the natural EOD (Bell and Russell, 1978). Smaller EOD mimic amplitudes were chosen for Figure 3 because their effects were cancelled relatively rapidly (within 1-2 hr), making it easier to study the significance of cancellation and negative images for prey detection. The effects of EOD mimics in these experiments are still within the range reported previously for the natural EOD. For Figures 4, 5, 6, and 7 EOD mimics were delivered locally through a dipole stimulus. The mimic used in these experiments was a previously recorded natural EOD waveform digitized, stored on a waveform generator (Rigol DG1022U) and presented through an analog stimulus isolation unit (SIU) (A-M systems, Model 2200). The peak-to-peak amplitude of the mimic measured at the output of the SIU was 8 μ A. Local delivery of the EOD mimic in these experiments minimized the possibility that spatial filtering could play a role in suppressing responses to the EOD mimic relative to prey-like stimuli. Local delivery of EOD mimics also made it possible to tightly connect electrophysiological measurements of prey-like stimulus detection performance with behavioral responses to prey-like stimuli. For local stimuli, behavioral novelty responses are presumably driven by a spatially restricted set of cells including those from which we recorded. This is not necessarily the case if the mimic is delivered globally since the entire ELL map is activated.

Prey-like Stimuli

Prey-like stimuli consisted of white noise to which a 5-20 Hz band-pass Butterworth filter was applied. Previous studies have shown that ampullary afferents in mormyrid fish respond well to stimuli within this frequency range (Engelmann et al., 2010). Sampling frequency was 10 kHz, and duration was 400 ms (Figure 2) or 2000 ms (remaining experiments). Stimuli were stored and delivered via a Cambridge Electronic Designs (Cambridge, UK) Power 1401 mkII device which performed digital to analog conversion. This signal was passed to an analog stimulus isolation unit (A-M Systems, Model 2200) which in turn was connected to a stimulating dipole (two Ag-AgCl balls 3 mm apart). For experiments in Figures 2 and 3 the dipole was positioned 1 cm from the skin using a spacer connected to the dipole. In the remaining experiments the dipole was positioned 1-2 mm from the skin. The amplitude of prey-like stimuli used in Figures 4, 5, 6, and 7 was 0.04 μ A peak-to-peak at the output of the stimulus isolation unit.

AP5 Injections

Micropipettes for pressure injections were constructed immediately preceding use using three-barrel glass pipette (1.2 mm OD per barrel, #3B120F-4, World Precision Instruments, Sarasota, FL) pulled to a long taper and tips broken to \sim 20 μ M under visual guidance. One barrel was filled with 1 mM APV in 0.9% saline, and the remaining barrels filled with saline, and 1 mM glutamate. In most experiments alexa 594 dextran was included in the pipette to allow for histological verification of the injection site. Prior to use, suitable ejection duration to deliver 15 nL at 20 PSI was calculated for each pipette barrel using previously described techniques (Bastian, 1993; Malpeli and Schiller, 1979). Typical ejection times were \sim 600 ms. After finding a suitable site for recording VLZ principal neurons, the location was noted, the recording pipette retracted, and the injection pipette tip placed at the recording pipette tip's point of entry. Basic trigonometric calculation was used to target a point 125 μ M lateral to the recording site to target the VLZ molecular layer. The recording pipette was reinserted, and neurons within \pm 100 μ m of the initial recording targeting site were recorded. Injection sites in the VLZ molecular layer were verified histologically using standard methods as described below.

Novelty Response Experiments

Experiments were performed in an isolation chamber. An open-bottomed chamber (60 \times 60 \times 60cm) was constructed from 1/4 inch plywood and lined with sound isolating open-cell foam. Following paralysis and resumption of spontaneous EOD commands, the chamber was lowered over the preparation and fish were allowed to adapt for 60 min before initiation of the experiment. Experiments shown in Figure 6 consisted of three 40 min periods in succession with each period consisting of 20 prey-like stimulus presentations.

Each presentation was 2 s in duration with an approximately 120 s interstimulus interval. Custom software was used to make delivery of a prey-like stimulus conditional on a stable EOD rate in the preceding 10 s. This was done to avoid spontaneous EOD accelerations from contaminating the results. Both the prey-like stimulus and the EOD mimic were presented via a local dipole situated over the face, between the eye and nares. The amplitude of the prey-like stimulus and the EOD mimic were identical to those used in the electrophysiological experiments shown in [Figure 4](#). Analysis included only those fish which the prey-like stimulus evoked an average command rate increase of >1.5 standard deviations above baseline during the initial command-alone period, as calculated by bootstrap analysis described below.

Modeling

We used a previously described model of negative image formation to simulate the effects of blocking associative synaptic depression on ELL neuron corollary discharge responses ([Kennedy et al., 2014](#)). Briefly, we modeled an ELL neuron as a passive, current-based leaky unit receiving excitatory input from 20,000 model granule cells ($r^i(t)$), with anti-Hebbian spike-timing-dependent plasticity at granule cell-ELL neuron synapses (w^i), and EPSPs fit to granule cell-evoked EPSPs recorded intracellularly ([Grant et al., 1998](#)). Because effects of AP5 were observed on responses to the command alone without an electrosensory stimulus, sensory input to the ELL neurons was not included in the model. The granule cell-ELL neuron learning rule has the form:

$$\dot{w}_i = \Delta^+ r^i(t) - \Delta^- \delta_{post}(t) \int_{-\infty}^t r^i(t') \zeta(t-t') dt'$$

$\delta_{post}(t) = 1$ if the ELL neuron spiked at time t , and 0 otherwise; $\zeta(t)$ determines the time dependence of associative depression. *In vivo* and *in vitro* recordings have demonstrated an anti-Hebbian synaptic plasticity rule in efferent cells of mormyrid and gymnotid fish ([Harvey-Girard et al., 2010](#)), although the exact timing dependence has not been characterized in mormyrids. We simulated the effects of pharmacological blockade of NMDA receptors by setting Δ^- to zero, i.e., turning associative depression off.

Histology

After recording, fish were deeply anesthetized with a concentrated solution of MS-222 (1:10,000) and brains removed and fixed in 4% paraformaldehyde for at least 24 hr. 60 μ M sections of ELL were cut on a cryostat or vibratome and a fluorescent microscope was used to visualize AP5 injection sites marked by Alexa 594 dextran.

QUANTIFICATION AND STATISTICAL ANALYSIS

Analysis of Spike Train Data

Electrophysiological data were digitized with a CED Power1401 MkII (Cambridge Electronic Design, Cambridge, UK) and analyzed in accompanying Spike2 software (v7.12c). Extracellular voltages were digitized at 20 kHz, and action potentials times extracted using the built-in peak-finding algorithm. Further analysis was performed in MATLAB using custom scripts.

ROC Analysis

Spike trains were smoothed with a 10 ms symmetrical Gaussian kernel to create a continuous firing rate. Maximum firing rate over the 100 ms period following either the EOD command in the case of command + mimic or command-alone periods, or the 100 ms period starting 4.5 ms before an EOD mimic delivered independent of the command. Only time windows within which no other EOD commands or mimics appeared were analyzed. Additionally, time windows which include the start or end of a prey-like stimulus were ignored. Analysis was performed using custom MATLAB scripts for calculating the ROC curve, and trapezoidal approximation was used to calculate the area under the ROC curve (AUC). See supplemental figures showing that results are qualitatively similar across a range of such periods from 10-300 ms. Additionally, performing the analysis over randomly chosen time points along the spike train, not locked to a command or mimic also shows qualitatively similar results.

Novelty Response Analysis

Novelty responses were quantified by taking the maximum EOD command rate during the 1 s following the onset of a prey-like stimulus presentation. A baseline rate was calculated by bootstrapping, as described below. Data are presented as deviation from this baseline. For bootstrapping we calculated the maximum command rate for all 1 s long segments in the experiments (spaced 200 ms apart, so overlapping by 800 ms) and used the mean of that as baseline, deviations from which are plotted as the command rate change ([Figures 6B and 7G](#)).

DATA AND SOFTWARE AVAILABILITY

Data and MATLAB code will be made available upon request.